JOURNAL OF THERMOPHYSICS AND HEAT TRANSFER
Vol. 23, No. 3, July–September 2009

Technical Notes

TECHNICAL NOTES are short manuscripts describing new developments or important results of a preliminary nature. These Notes should not exceed 2500 words (where a figure or table counts as 200 words). Following informal review by the Editors, they may be published within a few months of the date of receipt. Style requirements are the same as for regular contributions (see inside back cover).

Simple Model of Thermal Emission from Burning Aluminum in Solid Propellants

J. Harrison* and M. Q. Brewster†
University of Illinois at Urbana–Champaign, Urbana, Illinois 61801

DOI: 10.2514/1.39143

Nomenclature

A	=	surface area, m^2
$C(KL)$	=	optical-thickness correction factor
c_o	=	speed of light in vacuum, m/s
D	=	droplet diameter, m
F	=	geometric view factor
n	=	refraction index
K_a	=	absorption coefficient, 1/m
k	=	absorption index
L_m	=	mean beam length, m
L_{m0}	=	geometric mean beam length, m
r_{dc}	=	dc resistivity, $\mu\Omega \cdot$ cm
T	=	temperature, K
t	=	oxide-cap thickness, m
γ_D	=	Drude relaxation frequency, rad/s
ε	=	emissivity
ε_o	=	vacuum permittivity, $C^2/N \cdot m^2$
ε'	=	real part of complex dielectric constant
ε''	=	imaginary part of complex dielectric constant
θ	=	cap-orientation angle, deg
λ	=	wavelength, m
ρ	=	reflectivity
τ	=	transmissivity
Ω_p	=	plasma frequency, rad/s

Subscripts

Al	=	aluminum
Al_2O_3	=	aluminum oxide
cap	=	oxide cap
drop	=	droplet
ij	=	11,12,21, or 22
in	=	interface
tot	=	total
λ	=	spectral
1	=	interface between the oxide cap and Al droplet
12	=	paths between the oxide cap and the interface
21	=	paths between the oxide cap and the interface
22	=	paths between the oxide cap and itself

Received 16 June 2008; revision received 26 February 2009; accepted for publication 16 March 2009.

*Graduate Research Assistant, Mechanical Science and Engineering Department; hutystng29@gmail.com.

†H. G. Soo Professor, Mechanical Science and Engineering Department, 1206 West Green Street; brewster@uiuc.edu. Associate Fellow AIAA.

Introduction

THERE is a growing interest in and concern over accidental fires involving solid-propellant rocket motors. Many solid rocket motors are aluminized, and whether it is a large-scale launch booster or a smaller satellite orbital-transfer motor, fire spread in such situations would be significantly augmented by radiation from burning aluminum in the propellant. There is also a growing interest in improving computational fluid dynamics (CFD) modeling of internal flows in aluminized solid rocket motors, in which radiation can be a dominant energy-transport mechanism. Thus, there is a need for simple, accurate models of thermal emission properties of burning aluminum that can be incorporated in computational simulations of combustion of aluminized solid propellant.

Previous experiments [1] and analytical modeling [2] have shown that at 1–5 atm, infrared emission from burning aluminum is characterized by three distinct features: opaque surface emission from molten Al; optically intermediate volumetric emission from a molten Al_2O_3 cap that forms on the burning droplet; and oxide-smoke emission from an optically thin, detached, diffusion-flame envelope. This Note presents a simple mathematical model for emission by the first two contributions (Fig. 1). This description is useful in situations such as aluminized-propellant flowfield modeling, in which directional resolution of burning-droplet emission (oxide-cap orientation) may be important, but in which more detailed spatial resolution of emission from the droplet surface is not. It is simple enough to include in CFD codes and it is fast. If directional resolution is not required of the properties, it is even faster.

Model Discussion

The model is based on the assumption of uniform, diffuse radiosity (UDR) applied separately to each part of the burning droplet, metal, and oxide cap. For the opaque metal, this amounts simply to assuming diffuse, uniform surface emission. For the oxide cap, it means assuming diffuse, uniform volumetric emission. The burning droplet, metal, and oxide cap are assumed to be isothermal at 300 K below the boiling point of aluminum (2713 K at 1 atm) or 2413 K at 1 atm.

The droplet is treated as two distinct emitting regions: metal and oxide cap. The molten oxide cap is assumed to be a homogeneous, nonscattering, emitting, absorbing medium with the shape of a truncated sphere of the same diameter as the burning droplet D and thickness t oriented at an angle θ with respect to an observer (see Fig. 1).

Droplet emissivity is the sum of the contributions from the metal and oxide caps:

$$\varepsilon_{\lambda,\mathrm{drop}} = \varepsilon_{\lambda,\mathrm{Al}} \frac{A_{\mathrm{Al}}}{A_{\mathrm{tot}}} + \varepsilon_{\lambda,\mathrm{cap}} \frac{A_{\mathrm{cap}}}{A_{\mathrm{tot}}} \tag{1}$$

The fractional areas of the cap and aluminum are specified by the cap thickness-to-diameter ratio:

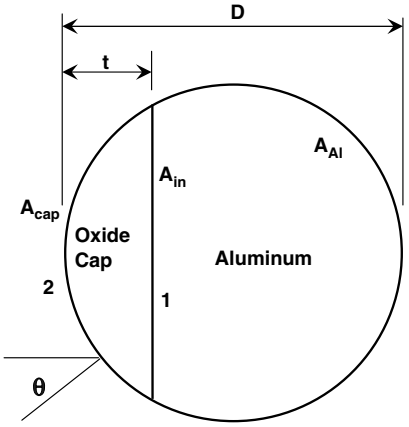

Fig. 1 Schematic diagram of burning aluminum droplet and oxide cap.

$$\frac{A_{\text{cap}}}{A_{\text{tot}}} = \frac{\pi Dt}{\pi D^2} = \frac{t}{D}, \qquad \frac{A_{\text{Al}}}{A_{\text{tot}}} = 1 - \frac{t}{D} \tag{2}$$

The spectral hemispherical (approximated as normal) emissivity of molten aluminum can be calculated from the optical constants as

$$\varepsilon_{\lambda,\text{Al}} = 1 - \frac{(n_{\text{Al}} - 1)^2 + k_{\text{Al}}^2}{(n_{\text{Al}} + 1)^2 + k_{\text{Al}}^2} \tag{3}$$

The spectral emissivity of the oxide cap, $\varepsilon_{\lambda,\text{cap}}$, is obtained from the (assumed uniform and diffuse) radiosity emerging from the oxide cap. Following standard analysis of UDR modeling for homogeneous nonscattering participating media [3], the cap emissivity is

$$\varepsilon_{\lambda,\text{cap}} = \varepsilon_{22,\lambda} F_{22} + \varepsilon_{21,\lambda} F_{21}(1 + \rho_{1,\lambda}\tau_{21,\lambda}) + \varepsilon_{1,\lambda}\tau_{21,\lambda} F_{21} \tag{4}$$

The first term accounts for volumetric emission along paths between the oxide-cap surface (surface 2) and itself. The second term is for volumetric emission along paths between the cap surface (surface 2) and the cap/Al interface (surface 1). It includes the contribution emitted directly to the environment and that reflected at the oxide/Al interface (surface 1), transmitted through the cap. The last term is for surface emission at the oxide/Al interface (surface 1). Reflection and refraction effects at the oxide-cap surface (surface 2) are not included (reflection can be added later). The geometric view factors are

$$F_{21} = F_{12}\frac{A_{\text{in}}}{A_{\text{cap}}} = 1 \cdot \frac{\pi[(D/2)^2 - (D/2 - t)^2]}{\pi Dt} = 1 - \frac{t}{D} = 1 - F_{22} \tag{5}$$

where A_{in} is the interface area. The mean transmittance and emittance factors through the oxide cap are

$$\tau_{ij,\lambda} = \exp(-K_{a\lambda} L_{m,ij}), \qquad \varepsilon_{ij,\lambda} = 1 - \tau_{ij,\lambda} \tag{6}$$

where the absorption coefficient is given in terms of the oxide extinction index as

$$K_{a\lambda} = \frac{4\pi k_{\text{Al}_2\text{O}_3}}{\lambda} \tag{7}$$

The path lengths (i.e., mean beam lengths) $L_{m,ij}$ are estimated from the geometric (optically thin) mean beam lengths using a smoothing transition function to account for the effects of optical thickness:

$$L_{m,ij} = C(KL) L_{m0,ij}$$

$$C(KL) = 0.9 + 0.1\left\{\frac{1}{1 + \exp[4(K_{a\lambda} L_{m0,ij} - 0.6)]}\right\} \tag{8}$$

The exponential transition function serves to make the value of the optical-thickness correction factor C go toward unity for optically thin conditions and toward 0.9 for optically thick conditions. Exact expressions for geometric mean beam lengths $L_{m0,ij}$ could be determined for this simple geometry; however, other approximations in the model do not warrant it. Instead, the geometric mean beam lengths $L_{m0,22}$ and $L_{m0,21}$ are taken as the same and equal to two-thirds of the cap thickness:

$$L_{m0,22} = L_{m0,21} = L_{m0} = \tfrac{2}{3}t \tag{9}$$

The spectral emissivity/absorptivity and reflectivity of the oxide/Al interface (surface 1) are obtained from the Fresnel relations as

$$\varepsilon_{1,\lambda} = 1 - \rho_{1,\lambda} = 1 - \frac{(n_{\text{Al}} - n_{\text{Al}_2\text{O}_3})^2 + k_{\text{Al}}^2}{(n_{\text{Al}} + n_{\text{Al}_2\text{O}_3})^2 + k_{\text{Al}}^2} \tag{10}$$

The optical constants of aluminum are taken from a dispersion theory model by Hüttner [4]. Hüttner's semiphenomenological approach follows the usual practice for polyvalent metals with almost free conduction electrons by including simple dispersion theory models of two types of nearly free electron transitions: 1) the Drude model for intraband transitions and 2) the Lorentzian model for interband transitions that arise as a consequence of the parallel-band effect. Aluminum has two interband transitions at wavelengths near 0.8 and 2–3 μm. The 0.8 μm band has weaker conductivity and absorption index but stronger film/layer absorption. For solid aluminum, both the intra- and interband transitions contribute to the optical constants in the near- and midinfrared regions; in the far-infrared region, interband-transition contribution is negligible. For liquid aluminum, intraband transitions dominate over the entire infrared spectrum. Because burning aluminum droplets are at temperatures well above the melting point, intraband transitions dominate the infrared optical properties. Figure 2 shows the optical constants for aluminum at the assumed burning-droplet temperature at 1 atm of 2413 K. The smooth monotonic character of the curves, without noticeable dispersion near the interband-transition wavelengths of 0.8 and 2–3 μm, is indicative of the dominance of intraband transitions. To a good approximation, the interband contributions could be neglected at this temperature and higher. In this case, the optical constants of aluminum are given by the following Drude model equations:

$$\varepsilon'_{\text{Al}}(\lambda, T) = 1 - \frac{\Omega_p^2}{\gamma_D^2(T) + (2\pi c_o/\lambda)^2} \tag{11a}$$

$$\varepsilon''_{\text{Al}}(\lambda, T) = \frac{\Omega_p^2 \gamma_D(T)}{(2\pi c_o/\lambda)\gamma_D^2(T) + (2\pi c_o/\lambda)^3} \tag{11b}$$

$$\Omega_p = 12.75 \text{ eV} = 1.94 \times 10^{16} \text{ rad/s} \tag{12}$$

$$\gamma_D(T) = \Omega_p^2 \varepsilon_o r_{\text{dc}}(T); \qquad \varepsilon_o = 8.85 \times 10^{-12} \text{ C}^2/\text{N} \cdot \text{m}^2 \tag{13}$$

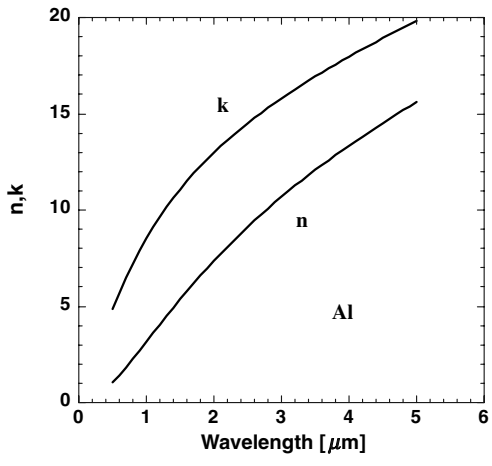

Fig. 2 Optical constants of molten aluminum at 2413 K.

$$r_{\mathrm{dc}}(T) = 24.23 + 0.0145(T\,[K] - 933)\ \mu\Omega \cdot \mathrm{cm} \qquad (14)$$

$$n_{\mathrm{Al}} = \left(\frac{\sqrt{\varepsilon'^2_{\mathrm{Al}} + \varepsilon''^2_{\mathrm{Al}}} + \varepsilon'_{\mathrm{Al}}}{2} \right)^{1/2} \qquad (15a)$$

$$k_{\mathrm{Al}} = \left(\frac{\sqrt{\varepsilon'^2_{\mathrm{Al}} + \varepsilon''^2_{\mathrm{Al}}} - \varepsilon'_{\mathrm{Al}}}{2} \right)^{1/2} = \frac{\varepsilon''_{\mathrm{Al}}}{2n_{\mathrm{Al}}} \qquad (15b)$$

The optical constants for molten aluminum as determined by the Drude model are thus primarily set by the dc-conductivity (or resistivity). A comparison of Hüttner's [4] relation for dc-resistivity in Eq. (14) with a variety of other researchers' results shows relatively little discrepancy between various sources. Thus, the optical constants of aluminum, albeit at elevated temperatures during combustion, are captured fairly accurately by the present model. The optical constants of Al_2O_3, on the other hand, show wide variation between different sources and experimental conditions [5–7].

The optical constants of Al_2O_3 used here and shown in Fig. 3 at 2413 K are taken from a combination of sources, with the primary source being Bakhir et al. [5]. This source was taken as the primary one because the experimental data used were for an aluminized mixed fuel (i.e., composite propellant). Data from aluminum oxide in other environments, such as hydrogen–oxygen flames or laser heating in various gases, show significant variation in the absorption index. Bakhir et al.'s conditions most closely resemble the present conditions of an aluminized composite propellant. Here, λ is in microns:

$$n_{\mathrm{Al_2O_3}} = \left[1 + \lambda^2 \left(\frac{1.02378}{\lambda^2 - 0.00377588} + \frac{1.058264}{\lambda^2 - 0.0122544} + \frac{5.280792}{\lambda^2 - 321.36164} \right) \right]^{0.5} \cdot \left[1 + 0.029 \left(\frac{T(K)}{1000} - 0.473 \right) \right] - 0.04 \qquad (16a)$$

$$k_{\mathrm{Al_2O_3}} = (0.001)(1 + 0.7\lambda + 0.06\lambda^2) \times \exp\{0.001847(T[K] - 2950)\} \qquad (16b)$$

The refractive index of Eq. (16a) is from Eq. (8) in [6] but shifted down by 0.04 to better match the data in Table 1 of [5] at 2950 K. The absorption index of Eq. (16b) is from Eq. (11) of [7], which is a fit to the data in Fig. 1 of [6] but reduced here by a factor of 2. These relations are not model-based, but are simply curve fits of experimental data. The monotonic-increasing behavior of the absorption index with wavelength in Fig. 3 is indicative of both visible/near-infrared free-carrier absorption and infrared phonon absorption, which dominate the absorption index in this region. Although some models include an upswing in absorption index at short wavelengths due to ultraviolet interband transitions, that feature is not included here.

Figure 3 also shows the absorption coefficient for aluminum oxide at 2413 K, the product of which with path length is optical depth, and the inverse of which is photon mean free path. The mean free path ranges from 100 to 200 μm, indicating that oxide caps, which typically range from 10 to 200 μm, are not optically thick, but optically intermediate, and thus exhibit path-length-dependent effects, as observed experimentally [1,2].

Figure 4 shows the calculated spectral-normal emissivity for both bare Al and the Al/Al_2O_3 (metal/cap) interface. These properties are relatively accurate and reliable, even for high-temperature combustion conditions. Compared with aluminum, the optical constants of aluminum oxide are much more dependent on the environment in which the aluminum burns. Certainly, there is need for further studies of aluminum oxide optical properties and effects of environment and composition. The present data, particularly for absorption index, should be viewed as being subject to change as better information becomes available.

All of the relations are defined to determine the droplet emissivity for a given droplet diameter and cap thickness. Directional emissivity can also be obtained by considering the fractions of oxide-cap and metal surface areas viewed by an observer for a particular cap-orientation angle using analytic geometry.

Results and Discussion

The directional-spectral (3.4 μm) droplet emissivity at 1 atm as a function of cap-orientation angle for a 200 μm droplet at 2413 K (1 atm) and a range of cap thicknesses is shown in Fig. 5. The influence of smoke emission is not included. The wavelength 3.4 μm corresponds to infrared measurements [1] from which oxide-cap parameters were developed previously via a detailed line-of-sight (LOS) analysis discussed elsewhere [2]. Results are shown in Fig. 5 for both the present UDR model and the LOS analysis for comparison. The lowest curves (horizontal lines, $t = 0$) of Fig. 5 are for pure metal (no cap); the emissivity is that of Al. The top curves (horizontal lines, $t = 200$ μm) are for pure oxide. The curves between $t = 50$, 100, and 150 μm are for varying cap thickness. The left side of Fig. 5 ($\theta = 0$) shows results for the cap facing toward the observer, the middle ($\theta = 90$ deg) is for the observer looking at the cap from the side, and the right ($\theta = 180$ deg) is the cap facing away from the observer. The enhancement in droplet emission for angles less than 90 is due to oxide-cap emission. As cap thickness increases, the emissivity increases not only because of increased relative cap surface area, but also because of increased optical depth in the cap. The values in parentheses are the integrated (over cap orientation)

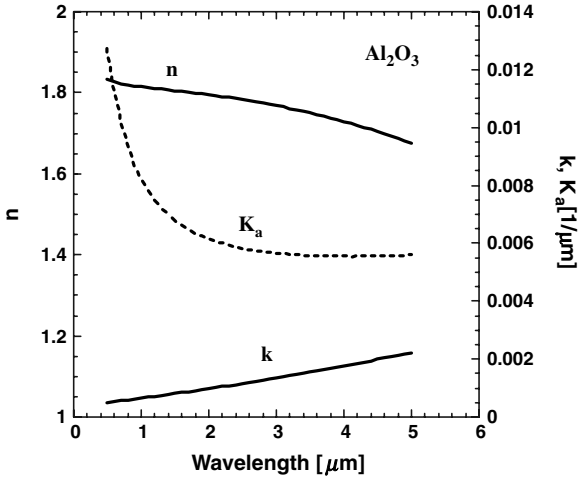

Fig. 3 Optical constants and absorption coefficient of molten aluminum oxide at 2413 K.

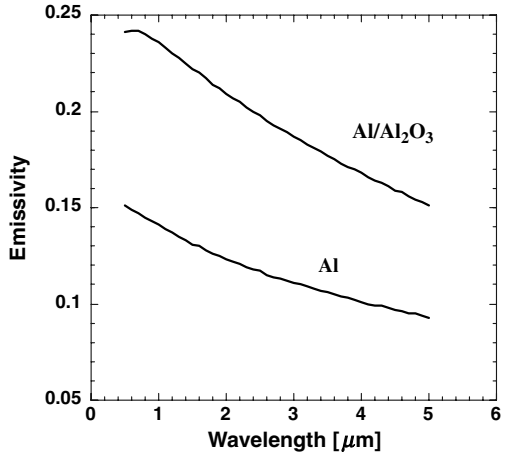

Fig. 4 Spectral emissivity of bare aluminum (Al) and metal/oxide-cap interface (Al/Al_2O_3) at 2413 K.

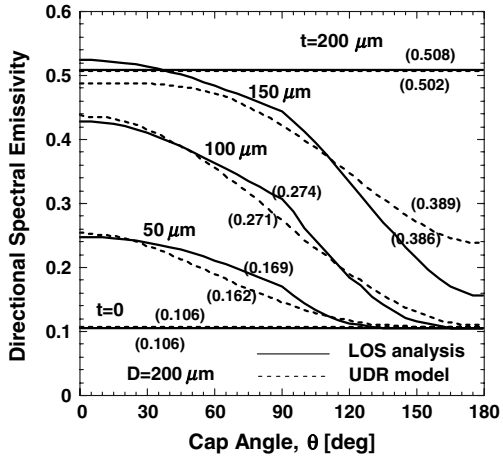

Fig. 5 Directional-spectral (3.4 μm) emissivity of a 200 μm burning Al/Al_2O_3 droplet at 2413 K (1 atm) for varying oxide-cap thickness by the UDR model and LOS analysis 2, ignoring oxide-smoke emission (directionally integrated emissivities in parentheses).

droplet emissivities, which can be obtained either by integrating the directional emissivities or directly from Eqs. (1–16) (the latter being much faster computationally). Agreement between the simpler UDR model and the more rigorous LOS analysis is generally good, particularly for integrated emissivities. The worst agreement for directional emissivity, up to 40% error, is for thick caps (150 μm) with the cap facing away (near 180 deg). This degree of disagreement is to be expected and is commensurate with the UDR model approximations. Still, even for the 150 μm cap, the integrated droplet emissivity of UDR is within a percent of LOS. The UDR model is a good compromise between computational speed and predictive accuracy.

Spectral emissivity (not directional, but over all cap orientations) is shown in Fig. 6 as a function of wavelength for a range of cap thicknesses for a 200 μm droplet at 2413 K. The enhancement in emissivity due to increasing oxide cap is strong over all wavelengths, but somewhat stronger at shorter wavelengths, due to the k/λ effect in the absorption coefficient.

Total emissivity integrated over wavelength and direction is shown in Fig. 7 as a function of droplet diameter for a range of cap thickness-to-diameter ratios t/D. For diameters above about 30 μm, the behavior with increasing t/D is similar to that described previously (for 200 μm). That is, increasing oxide cap increases total emissivity due to increasing oxide surface area and optical depth. For diameters less than 30 μm, the oxide cap is so optically thin that the trend is reversed: increasing t/D means eliminating metal that is actually a stronger emitter than the optically thin oxide material replacing it.

In complex numerical simulations, it is desirable to eliminate spectral integration and use effective gray properties if possible. Figure 7 shows results (discrete points) for a gray-property calculation (UDR gray model). If the proper wavelength is selected, close agreement with nongray results can be achieved. For conditions at 1 atm (2413 K), 1.6μm is the wavelength at which spectral and total properties are the same. At this wavelength, $n_{Al} = 5.78$, $k_{Al} = 11.6$, $n_{Al_2O_3} = 1.80$, $kAl_2O_3 = 0.000844$, $K_a = 0.00663\ 1/\mu$m, $\varepsilon_{Al} = 0.130$, and $\varepsilon_{Al/Al_2O_3} = 0.220$. For pressures higher (lower) than 1 atm and therefore higher (lower) droplet temperatures, the best effective gray wavelength would be slightly lower (higher), but could still be determined using the UDR nongray model (e.g., 1.2 μm at 3600 K). All of the results described to this point are for the metal/cap droplet only; the effect of detached-flame oxide-smoke emission is neglected.

The influence of smoke emission was estimated previously [2] using the LOS analysis. For a spherically symmetric burning droplet (ignoring oxide cap), the increase in droplet total emissivity due to flame-smoke emission at 1 atm was found to increase linearly with droplet diameter as $0.001D$ (in microns). The linearity is due to the optically thin nature of the smoke envelope. As cap thickness increases, there is less metal surface area exposed to burn and form oxide smoke. Thus, a reduction in smoke emission is in order with an oxide cap present. A reasonable approximation is to proportionately reduce the smoke-emission contribution by the relative surface area reduction of exposed metal $(1 - t/D)$, as shown subsequently.

At 1 atm, the UDR gray model, including oxide-smoke emission, is composed of the following relations for burning-droplet emissivity as a function of droplet size and oxide-cap thickness,

$$\varepsilon_{drop} = 0.130(1 - t/D) + \varepsilon_{cap}(t/D) + 0.001D[\mu m](1 - t/D) \quad (17)$$

$$\varepsilon_{cap} = 1 - \tau_{Al_2O_3} - (1 - 0.780\tau_{Al_2O_3})\tau_{Al_2O_3}(1 - t/D) \quad (18)$$

$$\tau_{Al_2O_3} = \exp(-0.00442Ct[\mu m]) \quad (19)$$

$$C = 0.9 + 0.1\left\{\frac{1}{1 + \exp(0.0177t[\mu m] - 2.4)}\right\} \quad (20)$$

which can readily be incorporated into a CFD code with little penalty in computational time. All that is necessary is to specify droplet size and oxide-cap thickness, which presumably can be given by an appropriate aluminum droplet combustion model, and cap-orientation effects (if any), which can be modeled according to the local velocity field.

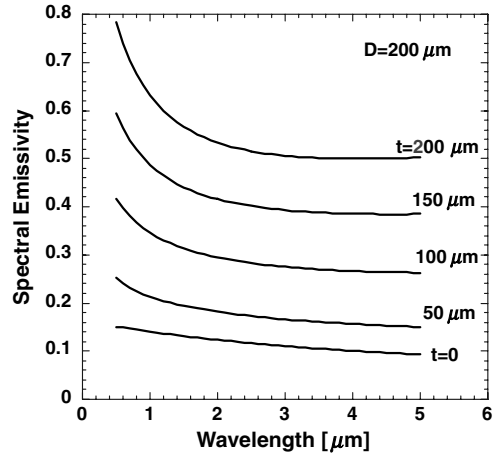

Fig. 6 Spectral emissivity (directionally integrated) of a 200 μm burning Al/Al_2O_3 droplet at 2413 K (1 atm) for varying oxide-cap thickness by UDR model, ignoring oxide-smoke emission.

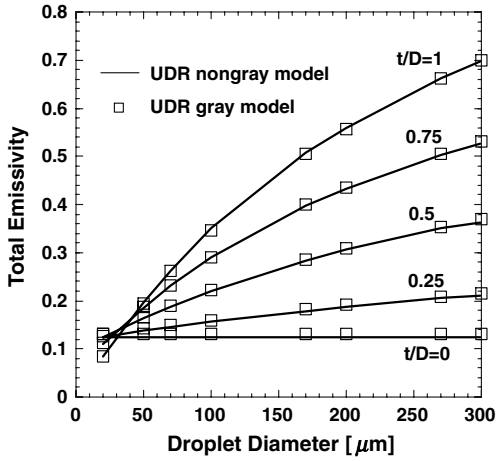

Fig. 7 Total emissivity (directionally and spectrally integrated) of burning Al/Al_2O_3 droplets at 2413 K (1 atm) for varying oxide-cap thickness by the nongray (lines) and gray (points) UDR model, ignoring oxide-smoke emission.

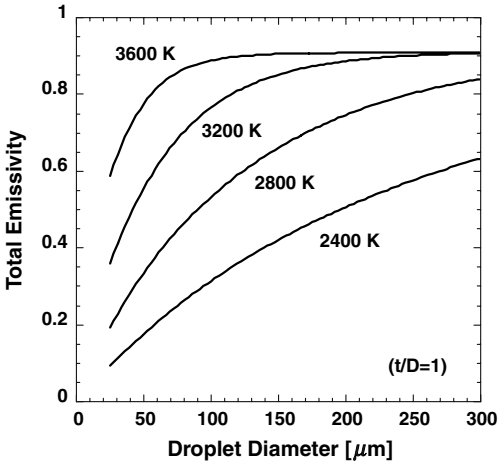

Fig. 8 Total emissivity of inert Al_2O_3 droplets by the nongray UDR model.

Although the UDR model was developed primarily for burning droplets, it can also be applied to inert oxide droplets left over after burnout of aluminum. In this case, the metal and oxide-smoke flame-envelope contributions vanish. The total emissivity is plotted in Fig. 8 as a function of droplet diameter for several temperatures. Once aluminum combustion ceases, the droplet temperature is no longer limited by the boiling point of aluminum, but is pulled toward the temperature of the surrounding gas, which may range from 2400 to 3600 K. In Fig. 8, the oxide-cap emissivity has been reduced (multiplied) by 1 minus the oxide-cap/gas interface (normal) reflectivity,

$$1 - \rho_{Al_2O_3} = 1 - \frac{(n_{Al_2O_3} - 1)^2}{(n_{Al_2O_3} + 1)^2} \tag{21}$$

which is slightly greater than 0.9 at these temperatures (0.92 for $\lambda = 1.6$ μm at 2400 K). If this reflection were not included, the droplet emissivity would (incorrectly) approach 1 for opaque conditions. Figure 8 shows that opaque oxide-droplet conditions occur for droplets greater than about 200 μm and temperatures above 3200 K. This reflection loss factor, which was not applied to the oxide-cap portion of the burning droplet (to maintain consistency with the LOS analysis), could easily be included for burning droplets as well.

Conclusions

The present model of radiant emission from burning aluminum has various strengths, weaknesses, advantages, and disadvantages. These strengths and weaknesses are particularly related to uncertainty and variations in droplet temperature and the chemical reducing/oxidizing nature of the environment gases. The aluminum emission part probably has the least uncertainty, at least to the degree that the droplet temperature is known. Aluminum is not so subject to variations. Because of its composition, the temperature sensitivity of its optical constants is fairly well known. The oxide-cap emission part is somewhat less certain, because the absorption index is so sensitive to temperature and composition and because the oxide composition is so variable, depending on the environment. Practically realizable variations in gas environment produce small changes in oxide stoichiometry that produce large changes in absorption index. This is an area that needs better understanding and further research. Still, the oxide-cap radiative model is reasonably fundamental and appropriate. Accurate cap emission predictions are mostly contingent on accurate absorption index and cap size information. The detached-flame oxide-smoke emission part is the least certain. In this work, flame emission has only been characterized at 1 atm and needs further work. Both additional experimental measurements are needed at elevated pressures and a fundamental model of the flame emission is needed. Thus, the overall burning-droplet model is targeted for atmospheric pressure in typical propellant combustion gases; additional work on smoke emission would be necessary to extend the model to higher pressures.

References

[1] Harrison, J., and Brewster, M. Q., "Infrared Emitted Intensity Measurements from Burning Aluminum Droplets in Solid Propellants," *Combustion Science and Technology*, Vol. 181, No. 1, 2009, pp. 18–35. doi:10.1080/00102200802415029

[2] Harrison, J., and Brewster, M. Q., "Analysis of Thermal Radiation from Burning Aluminum in Solid Propellants," *Combustion Theory and Modeling*, Vol. 13, No. 3, 2009, pp. 999–999. doi:10.1080/13647830802684318

[3] Brewster, M. Q., *Thermal Radiative Transfer and Properties*, Wiley, New York, 1992.

[4] Hüttner, B., "Optical Properties of Polyvalent Metals in the Solid and Liquid State: Aluminum," *Journal of Physics: Condensed Matter*, Vol. 6, No. 13, 1994, pp. 2459–2474. doi:10.1088/0953-8984/6/13/008

[5] Bakhir, L. P., Levashenko, G. I., and Tamanovich, V. V., "Refinement of the Imaginary Part of the Complex Refractive Index of Liquid Aluminum Oxide," *Journal of Applied Spectroscopy*, Vol. 26, No. 3, 1977, pp. 3778–383. doi:10.1007/BF00617450

[6] Anfimov, N. A., Karabadjak, G. F., Khmelinin, B. A., Plastinin, Y. A., and Rodionov, A. V., "Analysis of Mechanisms and Nature of Radiation from Aluminum Oxide in Different Phase States in Solid Rocket Exhaust Plumes," 28th AIAA Thermophysics Conference, Orlando, FL, AIAA Paper 93-2818, July 1993,

[7] Reed, R. A., and Calia, V. S., "Review of Aluminum Oxide in Rocket Exhaust Particles," 28th AIAA Thermophysics Conference, Orlando, FL, AIAA Paper 93-2819, July 1993.